



COLLAPSE BEHAVIOR OF STEEL COLUMNS AS PART OF STEEL FRAME BUILDINGS: EXPERIMENTS AND NUMERICAL MODELS

Y. Suzuki⁽¹⁾, D.G. Lignos⁽²⁾

⁽¹⁾ Nippon Steel and Sumitomo Metal Corporation, suzuki.s2k.yusuke@jp.nssmc.com

⁽²⁾ Associate Professor, Swiss Federal Institute of Technology, Lausanne (EPFL), dimitrios.lignos@epfl.ch

Abstract

Earthquake-induced collapse risk assessment of steel frame buildings requires the use of deterioration models that simulate instabilities that cause strength and stiffness deterioration of structural steel components. In the case of steel columns in addition to cyclic deterioration in flexural strength, such models should capture the axial load – bending interaction, the axial contraction as well as the axial strength deterioration after the formation of local buckling within the column cross-section. Based on the available literature, experimental data that characterizes the hysteretic behavior of steel columns at large deformations is scarce. Therefore, the validation and further refinement of new or available steel column deterioration models becomes challenging.

This paper discusses the main findings of an extensive experimental program that characterized the hysteretic behavior of wide-flange and hollow structural steel (HSS) columns. The effect of various types of lateral loading protocols on the hysteretic behavior of steel columns was examined with nominally identical specimens. It is shown that a primary failure mode observed in steel columns is the axial shortening. The amount of axial shortening can be considerably different in end columns compared to that observed in interior columns within the same story of a steel moment-resisting frame (MRF). Symmetric loading protocols that are typically used for experimental testing of structural components provide insufficient information for modeling the cyclic deterioration in flexural strength and stiffness of steel columns near collapse. A fiber-based deterioration model is developed for HSS columns that is able to simulate the cyclic hardening prior to the formation of local buckling and the steel column post-buckling behavior including axial shortening. The proposed model is validated with steel column test data that became available from the experimental program.

Keywords: Steel columns, Collapse experiments, Deterioration modeling, Dynamic instability



1. Introduction

In the context of Performance-Based Earthquake Engineering (PBEE) it is essential to develop methods in order to reliably predict the collapse resistance of our building infrastructure. This can facilitate the quantification of building response parameters (i.e., strength reduction factors, system overstrength) that can be used in new construction as well as the utilization of new lateral load-resisting systems that minimize structural damage. Earthquake-induced collapse due to sidesway instability of a frame building occurs when one or a number of its stories displace sufficiently such that their story shear resistance becomes zero due to P-Delta effects and component deterioration in strength and stiffness. Several researchers have pointed out the need of component deterioration models to facilitate the collapse prediction effort [1,2]. In steel frame buildings with moment-resisting frames (MRFs) such models should capture the component deterioration due to local and global instabilities and/or fracture due to low cycle fatigue. Historically, a number of phenomenological models were employed for this purpose [1,3]. These models were calibrated with large sets of full-scale experimental data [4,5]. As part of this process, a fundamental problem has been the lack of data at large deformations as well as the influence of the employed lateral loading protocol on cyclic deterioration in strength and stiffness of a structural component [6]. In the case of steel columns due to lack of experimental data several issues related to their collapse behavior have been neglected or not properly understood. Few of these issues relate to (a) the coupling of axial load and bending due to lateral deformations; (b) the axial load variation due to dynamic overturning effects; and (c) the column axial shortening due to axial strength deterioration in addition to flexural strength of the member.

This paper first discusses the findings of an extensive large-scale experimental program that is conducted to address the collapse behavior of steel columns in steel frame buildings. The goal of the testing program is to characterize the hysteretic behavior of hollow structural steel (HSS) and wide-flange (W-shape) columns under various lateral-loading histories coupled with constant and varying axial load. The former and the latter represent the loading conditions of an interior and end steel column within an MRF, respectively. In particular, the effect of cross-sectional slenderness ratio on the cyclic deterioration in the flexural and axial strength of steel columns is examined. Based on the testing program, a high-fidelity component deterioration model is developed for HSS columns. In brief, the proposed model is able to capture (a) the coupling between the column axial force and flexural strength; (b) the effects of cyclic hardening prior to the onset of cross sectional local buckling; and (c) the column post-buckling behavior under various loading histories. The proposed model is implemented in an open-source finite element software for nonlinear response history analysis (NRHA) of steel frame buildings.

2. Steel column collapse experiments

In order to characterize the collapse behavior of steel columns subjected to large deformations associated with structural collapse an experimental program is carefully designed. In total, this program involves 21 HSS and W-shape steel columns that are subjected to a range of lateral loading protocols coupled with representative axial load ratios (see Section 2.1). The experimental setup (see Section 2.2) allows for column testing at very large deformations (i.e., 20% radians) till complete loss of the axial and/or flexural carrying capacity of a specimen is reached. The following subsections provide details regarding the test matrix, the employed loading protocols as well as the test setup. Finally, selective findings from the experiments are presented.

2.1 Test matrix

The experimental program involves 21 cantilever steel columns that are summarized in Table 1. From this table, three types of W-shapes (i.e., W14x53, W14x61 and W14x82) and two types of HSS shapes (i.e., HSS254x9.5 and HSS305x16) are tested. The W-shape columns are fabricated by ASTM A992 Gr. 50 steel (i.e., nominal yield stress, $f_y=345\text{MPa}$). The HSS columns are fabricated by ASTM A500 steel (i.e., nominal yield stress, $f_y=315\text{MPa}$). In order to examine the effect of cross-sectional compactness on the hysteretic behavior of the steel columns both types of cross-sections have practically the same span-to-depth-ratio, L/d (i.e., d is the cross-section depth). The W14x61 cross-section is slightly above the current compactness limits for highly ductile members based on AISC 341-10 [7]. The W14x82 is a highly ductile member based on [7]. The W14x53 cross-section has a narrow flange compared to that of the other two shapes. In all three cases, the global slenderness ratio, L/r_y (in which, L is the



column length and r_y is the radius of gyration with respect to the column cross-section's weak axis) is in the order of 37 such that lateral torsional buckling does not become a controlling failure mode. Similarly, the HSS254x9.5 shape has a local slenderness ratio, $D/t = 26.7$, which is below the limit for highly compact members as per [7]. The HSS305x16 shape is considered to be highly compact (i.e., $D/t = 19.1$) and is typically used in high-rise steel construction in Japan. The selected cross-sections allow for the assessment of the effect of local cross-sectional slenderness on the hysteretic behavior of steel columns.

Table 1 - Testing matrix

Designation	Section	Width-to-thickness		Span-to-depth ratio, L/d	Loading Protocol	
		b/t_f	h/t_w		Lateral	Axial
W-6-34-M-C	W14x53	6.1	34.1	5.2	Monotonic	Constant
W-6-34-S-C					Symmetric	Constant
W-6-34-C1-C					Near collapse C1	Constant
W-6-34-C1-V						Varying
W-6-34-C2-C					Near collapse C2	Constant
W-6-34-C2-V						Varying
W-8-34-S-C	W14x61	7.7	33.7	5.2	Symmetric	Constant
W-8-34-C1-C					Near collapse C1	Constant
W-8-34-C1-V						Varying
W-6-25-S-C	W14x82	5.9	24.6	5.0	Symmetric	Constant
W-6-25-C1-C					Near collapse C1	Constant
W-6-25-C1-V						Varying
H-27-M-C	HSS254x9.5	26.7		6.0	Monotonic	Constant
H-27-S-C					Symmetric	Constant
H-27-C1-C					Near collapse C1	Constant
H-27-C1-V						Varying
H-27-C2-C					Near collapse C2	Constant
H-27-C2-V						Varying
H-19-S-C	HSS305x16	19.1		6.0	Symmetric	Constant
H-19-C1-C					Near collapse C1	Constant
H-19-C1-V						Varying

From Table 1, the last varying parameter that is considered is the employed loading protocol. The W14x53 and HSS254x9.5 specimens are subjected to six different loading protocols. The first and second one involve monotonic and symmetric cyclic lateral loading protocol, respectively, coupled with constant compressive axial load. The third and fourth specimens are subjected to collapse-consistent lateral loading protocols coupled with constant compressive and varying axial load demands, respectively. Figure 1 shows an example of such loading protocol developed by Suzuki and Lignos [8,9]. From Figure 1a, the collapse-consistent loading protocol starts with small inelastic cycles followed by a large monotonic push. This represents the ratcheting behavior of a steel column in a steel MRF prior to collapse. If the column does not lose its stability, the protocol is repeated with an offset as shown in Figure 1a. To assess the differences between interior and end columns in steel MRFs varying and constant axial load is coupled with the lateral loading protocol. Figure 1b shows the axial load variation for an end column that ranges from $0.5P_y$ (P_y is the axial yield strength of the steel column) in compression to $-0.2P_y$ in tension due to dynamic overturning effects during the ground motion history. Note that the range of the variation is reduced with the number of inelastic cycles due to force redistribution in adjacent columns after the occurrence of local buckling. From Figure 1b, the load variation stabilizes once local buckling wave stabilization occurs within a steel cross section.

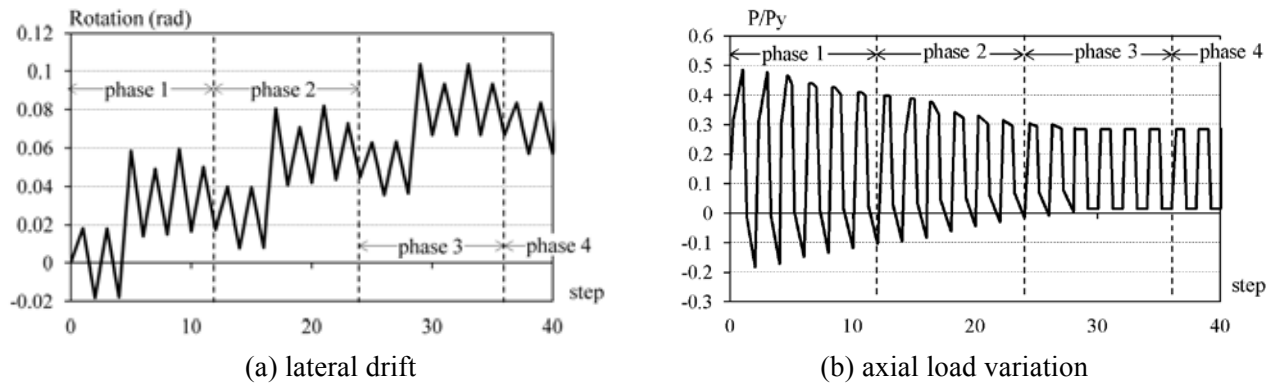


Fig. 1 – Typical near-collapse loading protocol for end columns (illustration for W14x53 steel column as adopted from [8])

In order to assess the effect of inelastic lateral loading cycles on the collapse-consistent protocol, specimens five and six are subjected to a long-duration near-collapse lateral loading protocol coupled with constant and varying axial load ratios, respectively. The W14x61, W14x82 and HSS305x16 specimens are only subjected to a symmetric lateral loading protocol with constant axial load as well as the collapse protocol that represents near-fault ground motions coupled with constant and varying axial load ratios.

2.2 Experimental setup

Figure 2 illustrates the test setup that is designed for experimental testing of cantilever steel columns. The specimens are idealized with fixed-pin boundary conditions (i.e., constant inflection point assumption). A 1,000kN/500mm long stroke dynamic actuator is employed in order to apply the lateral deformations to a test specimen. A 12,000kN vertical actuator is utilized to apply the constant and/or varying axial load on a steel column. The vertical actuator has a 300mm displacement stroke. From Figure 2, the axial load is applied to the column through an axially rigid link. The bottom end of the rigid link is connected to a structural pin, which is also connected to a test specimen through a 50mm thick steel adapter plate. A loading plate adaptor is connected to the pin and the lateral actuator in order to transfer the lateral displacement at the top of a test specimen. A steel column is fixed to the test bed through a 75mm thick base plate that is designed to remain elastic. Laterally bracing is employed in order to prevent any out-of-plane movement of a test specimen during testing.

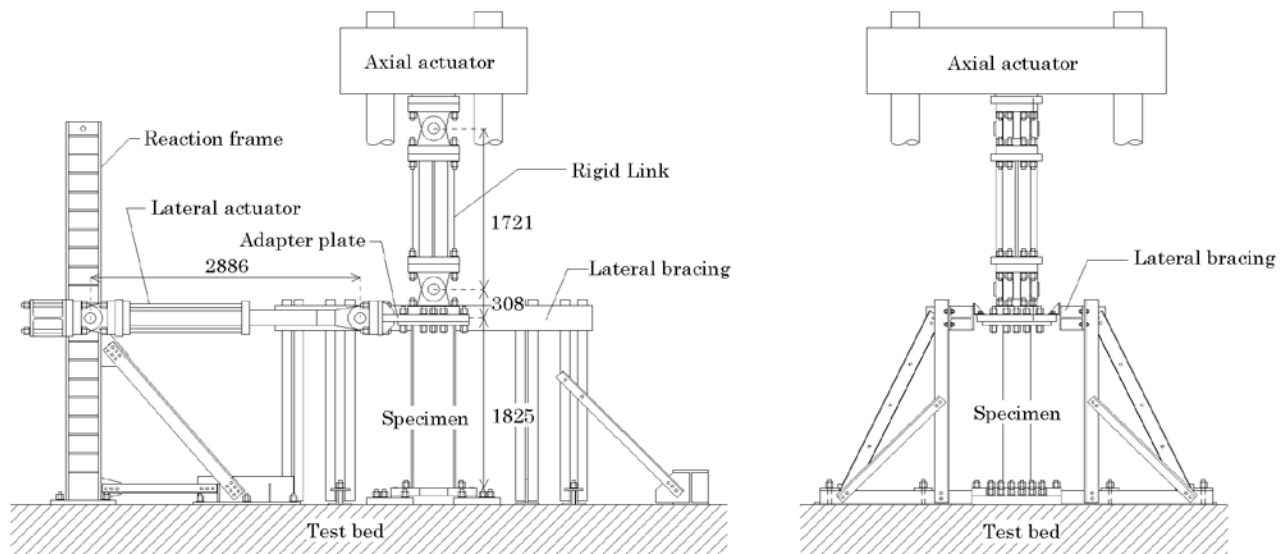
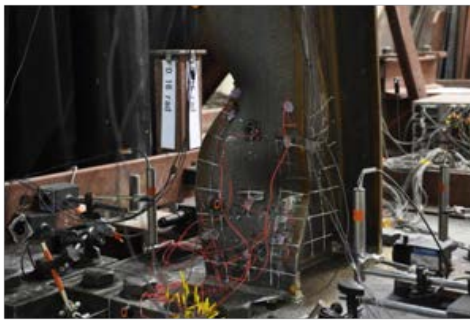


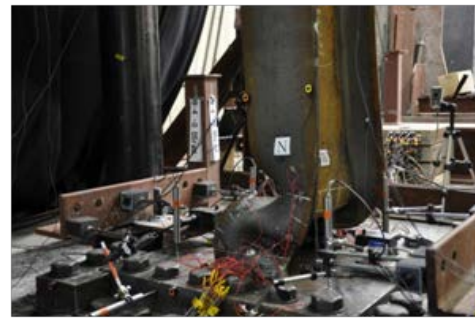
Fig. 2 –Setup for large-scale experimental testing of steel columns (dimensions in mm)

2.3 Test results and discussion

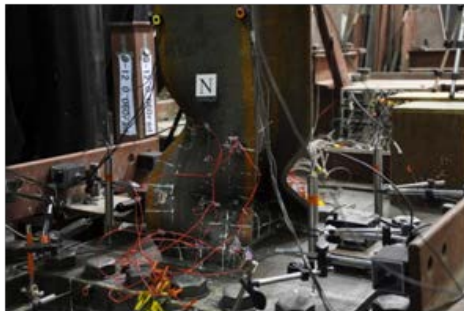
Figures 3 and 4 illustrate the observed failure modes near the fixed end of a W-shape and a HSS column, respectively, under various types of loading protocols. For W-shape columns subjected to constant compressive axial load, flange and/or web local buckling formed at $0.5d$ from the top of the column base regardless of the employed lateral loading protocol as shown in Figures 3a to 3c. From the same figures, at a later stage of the employed lateral loading history, a second local buckling wave formed at about $1.0d$ from the top of the column base. This triggered lateral torsional buckling at large deflections (i.e., larger than 6% radians). In all cases that the axial compressive load was kept constant, the steel columns experienced severe axial shortening. Figure 3d shows the plastic hinge formation of the same W-shape column subjected to varying axial load at 6% lateral drift ratio. Due to the axial load variation, most of the plastic deformation due to local buckling concentrated on one side of the steel column flange. This suggests that end columns experience smaller cumulative damage on their buckled flange compared to interior columns within the same story.



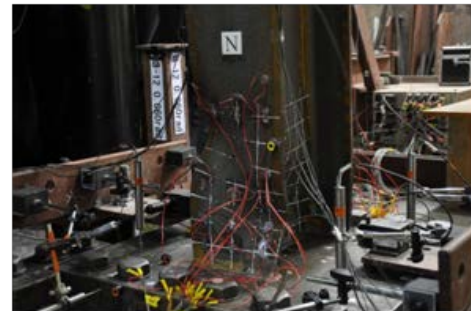
(a) W-6-34-M-C (16% drift)



(b) W-6-34-S-C (6% drift)



(c) W-6-34-C1-C (6% drift)



(d) W-6-34-C1-V (6% drift)

Fig. 3. Failure modes of W14x53 steel column under various loading protocols

Similarly, HSS columns subjected to constant compressive axial load developed a first local buckling wave at about $0.6d$ from the column base as shown from Figures 4a to 4c. For the case of varying axial load (See Figure 4d), the local buckling wave center developed at approximately $0.7d$. This is attributed to the second order moment demands. Note that the more compact HSS column (i.e., HSS305x16) developed the local buckling wave center at $1.1d$. This suggests that the assumption of point plastic hinge location at the end of the member is an abrupt approximation. HSS columns did not experience any twisting as expected. However, their hysteretic behavior was also characterized by severe axial shortening. It is worth mentioning that specimen H-27-S-C completely squashed at the first cycle of the 4% drift amplitude when it was subjected to a symmetric cyclic lateral loading protocol as shown in Figure 4b.

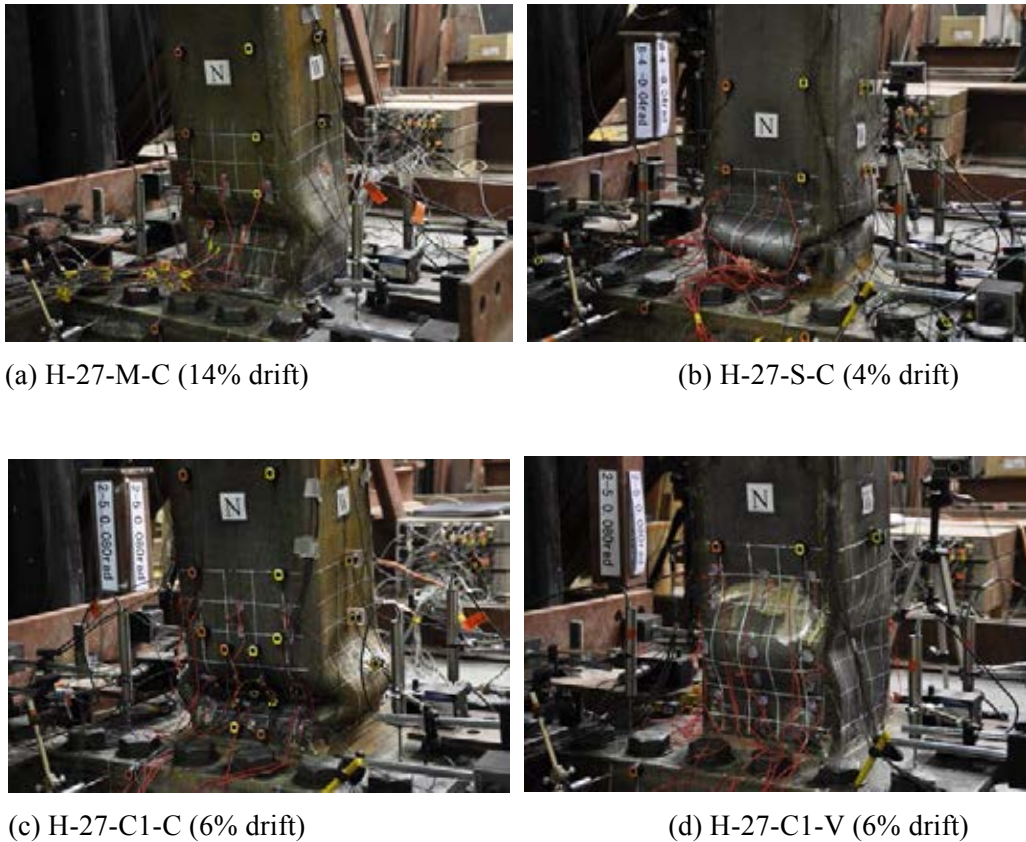


Fig. 4. Failure modes of HSS254x9.5 steel column under various loading protocols

Figures 5a and 5b compare the deduced moment versus chord rotation of the W14x53 and HSS254x9.5 specimens, respectively, under various lateral loading protocols. From this figure, the flexural strength deterioration of both specimens became zero at chord rotations larger than 15% based on the monotonic backbone curve. In addition, the flexural strength for both specimens deteriorated in the positive and negative loading direction when the axial load was kept constant. This is due to the formation of local buckling in both flanges of the steel columns. Note that when varying axial load is coupled with lateral drift demands then the flexural strength of a steel column does not typically deteriorate in the negative loading direction. This is due to the position of the cross-sectional neutral axis. Therefore, it is expected that interior steel columns would typically lose faster their flexural strength and axial load carrying capacity compared to end columns within the same MRF story.

From Figure 5, when a symmetric cyclic lateral loading protocol is employed the steel column flexural strength deteriorates a lot faster than a nominally identical specimen that experiences a collapse-consistent loading protocol. This is due to the large number of inelastic loading cycles included in a symmetric cyclic lateral loading protocol. However, columns in steel MRFs subjected to ordinary or near-fault ground motions would typically experience few inelastic cycles followed by a large monotonic push prior to structural collapse [6,10]. Prior studies associated with the collapse assessment of frame buildings have highlighted that the pre- and post-capping plastic rotation capacities are fundamental quantities for the reliable collapse assessment [1,11]. From Figure 5, this information becomes available only when a combination of a monotonic and a collapse-consistent lateral loading protocol is employed for experimental testing of steel columns. Same findings hold true for the rest of the tested specimens.

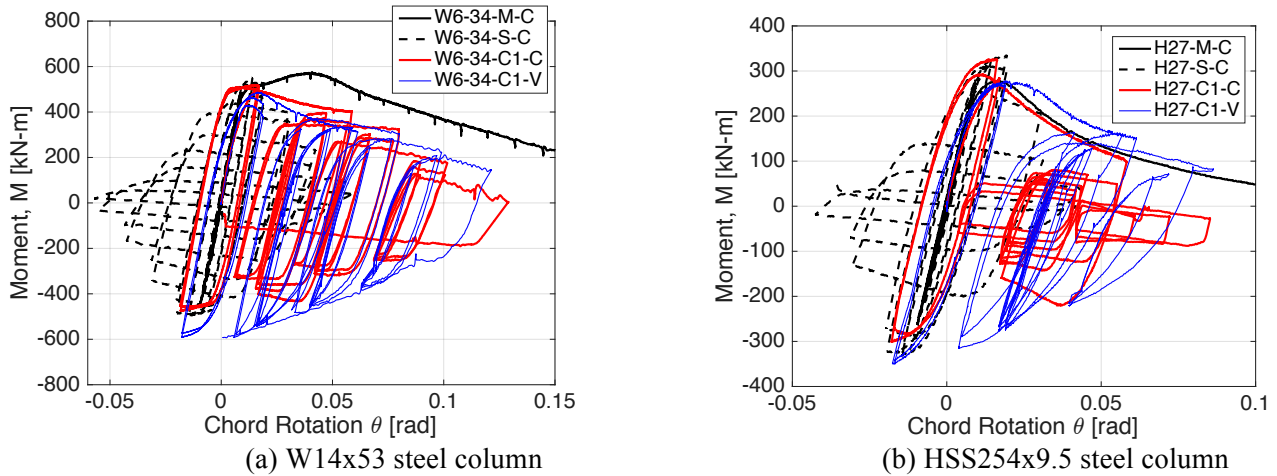


Fig. 5. Comparison of moment-rotation relations for nominally identical steel columns under various loading protocols

Figure 6 illustrates the steel column axial shortening versus chord rotation relations for the two steel columns discussed previously. In this figure, the axial shortening is normalized with respect to the column height. From Figure 6, when a constant compressive axial load is applied on a steel column its axial shortening accumulates in both the positive and negative loading directions regardless of the cross section shape. The amount of axial shortening depends on the number of inelastic loading cycles of the respective lateral loading protocol as well as the applied axial load. In particular, an end column would experience 6 to 7 times smaller axial shortening compared to an interior column. The reason is that an end column experiences tensile load in the negative loading direction due to dynamic overturning effects. From Figure 6, the axial shortening for end columns experiencing varying axial load demands varies linearly with respect to the chord rotation. From Figure 6b note that when for a given rotation the column axial shortening instantaneously amplifies the steel column loses its axial load carrying capacity. It is understood that column axial shortening is a failure mode that has not gained attention in current seismic design provisions. However, this failure mode is likely to cause tensile axial load demands in addition to flexure at a fully-restrained beam-to-column moment connection near the end column. This is due to the expected differential axial shortening between adjacent columns within the same MRF story. In order to limit the amount of column axial shortening an obvious solution can be the reduction of the local slenderness limits for highly ductile members [12,13].

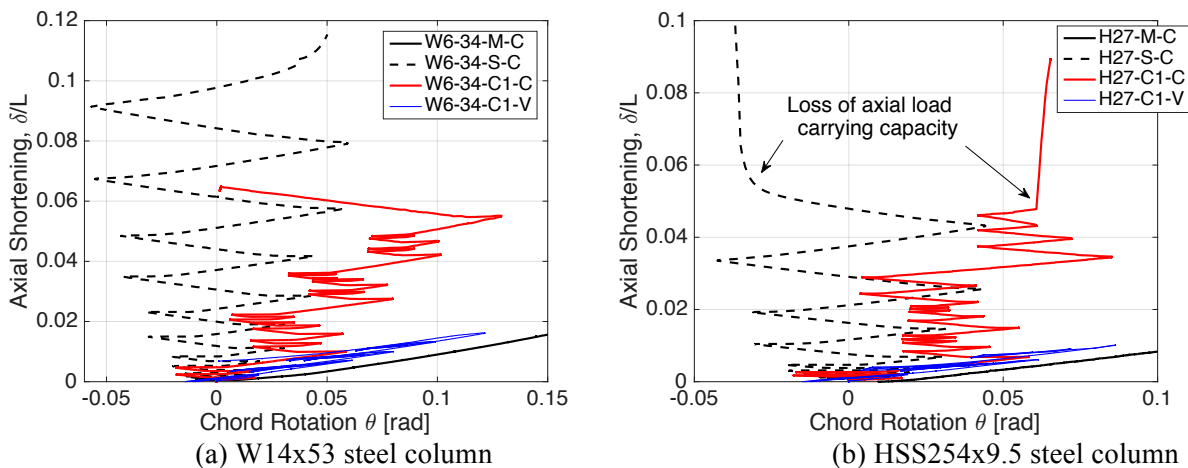


Fig. 6. Comparison of the axial shortening-rotation relations for nominally identical steel columns under various loading protocols

3. Proposed deterioration model for HSS columns

In an effort to realistically simulate the hysteretic behavior of HSS steel columns subjected to cyclic loading we propose a new deterioration model that captures the observed cyclic hardening in the post-yield range of a steel column prior to the onset of local instabilities within the cross-section. The same model is able to adequately simulate the steel column post-buckling behavior. For this purpose, a fiber-based approach is adopted that combines an engineering stress-strain constitutive relation assigned to a fiber cross-section within a force-based beam-column element formulation. The following sections briefly describe the deterioration model development including validation studies based on rigorous finite element analyses and the experimental data discussed in Section 2.

3.1 Modeling of cyclic hardening and post-buckling behavior

In order to capture the effect of cyclic hardening on the hysteretic behavior of a steel column the evolution law proposed by Lemaitre and Chaboche [14]. This model combines a nonlinear kinematic and an isotropic hardening component based on the following two equations,

$$\dot{\alpha} = C \frac{1}{\sigma^o} (\sigma - \alpha) \dot{\epsilon}_{pl} - \gamma \alpha \dot{\epsilon}_{pl} \quad (1)$$

$$\sigma^o = \sigma^o|_0 + Q_\infty (1 - e^{-b\epsilon_{pl}}) \quad (2)$$

in which, C is the initial kinematic hardening modulus, γ is the parameter, which determines the rate at which C decreases while ϵ_{pl} increases and α is the backstress; Q is the maximum change in the size of the yield surface. The parameter b defines the rate at which the size of the yield surface changes as ϵ_{pl} develops. Such parameters can be computed based on standard round coupons subjected to uniaxial tensile and cyclic loading as discussed in [12]. Figures 7a and 7b illustrate an example of the monotonic and cyclic stress-strain relation for a steel material, respectively. From Figure 7b, the numerical model is able to capture well the effect of cyclic hardening on the hysteretic behavior of the steel material. A more round hysteresis can be achieved with the use of more backstresses.

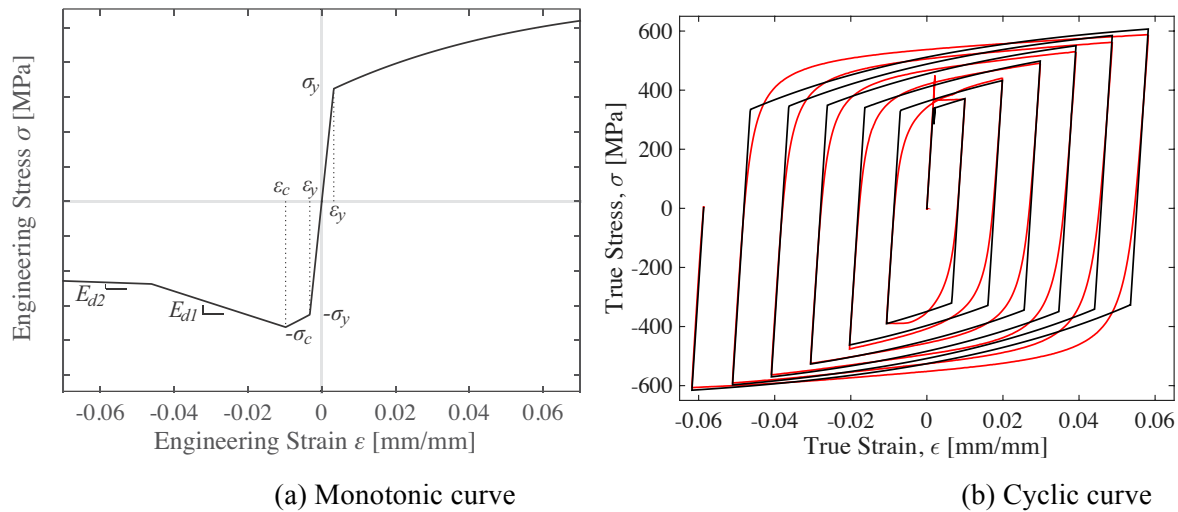


Fig. 7. Uniaxial monotonic and cyclic stress-strain relation for a steel material

In order to simulate the post-buckling behavior of HSS columns, a softening branch is considered within the uniaxial stress-strain relation that characterizes the monotonic axial compressive response of the steel material as shown in Figure 7a. The elastic and post-yield regions are defined based the material yield stress, σ_y and the Young's modulus, E based on a standard tensile coupon test. The post-buckling region initiates at an engineering strain ϵ_c and a capping engineering stress, $\sigma_c < \sigma_u$, and progresses with a negative slope E_{d1} as shown in Figure 7a.

At 50% of σ_c a second negative slope, E_{d2} is defined as shown in the same figure. This slope is typically smoother than E_{d1} . This represents the post-capping deterioration slope after stabilization at large strains as discussed in Krawinkler and Zohrei [15]. The equivalent uniaxial stress-strain curve of the steel material can be defined based on standard stub column compressive tests. Figures 8a and 8b show the proposed equivalent engineering stress-strain relation as deduced from uniaxial cyclic testing of HSS400x19 stub columns (noted as predicted) based on incremental and constant strain loading amplitude protocols. The equivalent strain is extracted from the buckled region within the stub column compressive test and in this case was $0.9d$. This length can be considered stable as discussed in Yamada et al. [16]. This assumption has been also validated by the authors with additional finite element studies. Superimposed in the same figure is the same relation as deduced from stub column finite element analysis (noted as measured). From this figure it is evident that the proposed material model is able to simulate the equivalent stress-strain relation of HSS columns relatively well.

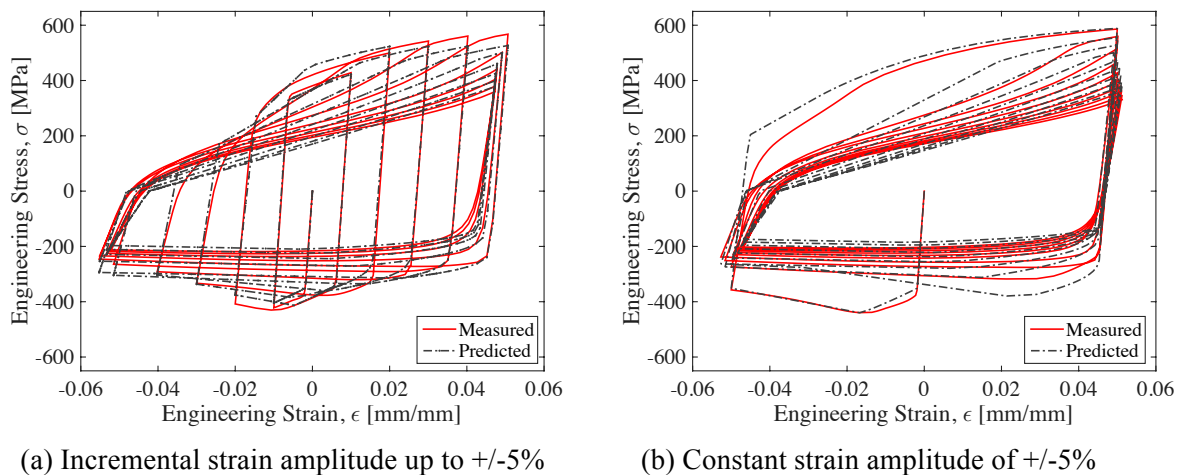


Fig. 8. Equivalent stress-strain relation of HSS400x19 stub column

The proposed equivalent stress-strain material model is assigned to a fiber element that is used to discretize an HSS cross-section. In order to achieve a balance between simulation accuracy and computational workload a number of discretization schemes were examined. Few of those are shown in Figure 9a. For two dimensional simulations, the section discretization perpendicular to the loading direction is not relevant. This is not valid for three-dimensional simulations. Based on parametric studies, a 16-12-13 HSS section discretization (i.e., 1x6 fibers in the web, 1x2 fibers in the flange and 1x3 fibers in the corner portion) is a reasonable compromise between computational efficiency and accuracy for two dimensional collapse simulations.

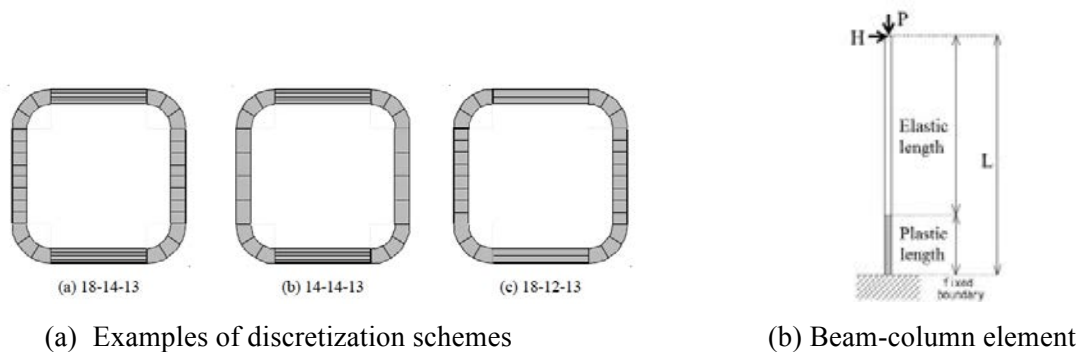


Fig. 9. Fiber-based nonlinear beam-column element

The fiber cross-section is utilized within a force-based plastic hinge frame element (See Figure 9b) based on a force-based element formulation [17]. The mid-point integration scheme [18] is employed. A force-based formulation is preferred over a displacement-based one because in the former the internal

element interpolation functions represent accurately the force equilibrium with just one element [19] compared to the latter. The mid-point integration scheme is selected because the maximum flexural demands within the column typically occur at a distance of $0.4d$ to $0.5d$ away from the column base as discussed in Section 2. This is due to the second order moment demands because of the presence of the compressive axial load. In Figure 9b, a plastic hinge length equal to the respective HSS column depth d is typically a good approximation.

3.2 Preliminary validation with experimental data

This section discusses the validation of the proposed deterioration model for simulating the hysteretic behavior of HSS columns under cyclic loading. This is achieved through a comparison with the experimental data on HSS columns discussed in Section 2. Figure 10 shows a comparison of the predicted versus measured moment-rotation relation of the HSS305x16 under a symmetric cyclic and collapse-consistent loading protocol. From this figure, the proposed model is able to simulate reasonably well the cyclic hardening of a steel column prior to the formation of local buckling. In addition, the proposed model captures the cyclic deterioration in flexural strength of the steel column regardless of the employed loading history. From Figure 10b, at large deformations (i.e., larger than 12% radians) the proposed model slightly over predicts the flexural strength of the column. This is attributed to the fact that the corner portion of the HSS section has different material properties than its flat portion due to the rolling process of the cross section. For simplicity, this was neglected as part of the preliminary evaluation of the proposed model discussed in this paper but can be easily considered in a more refined version of the proposed model.

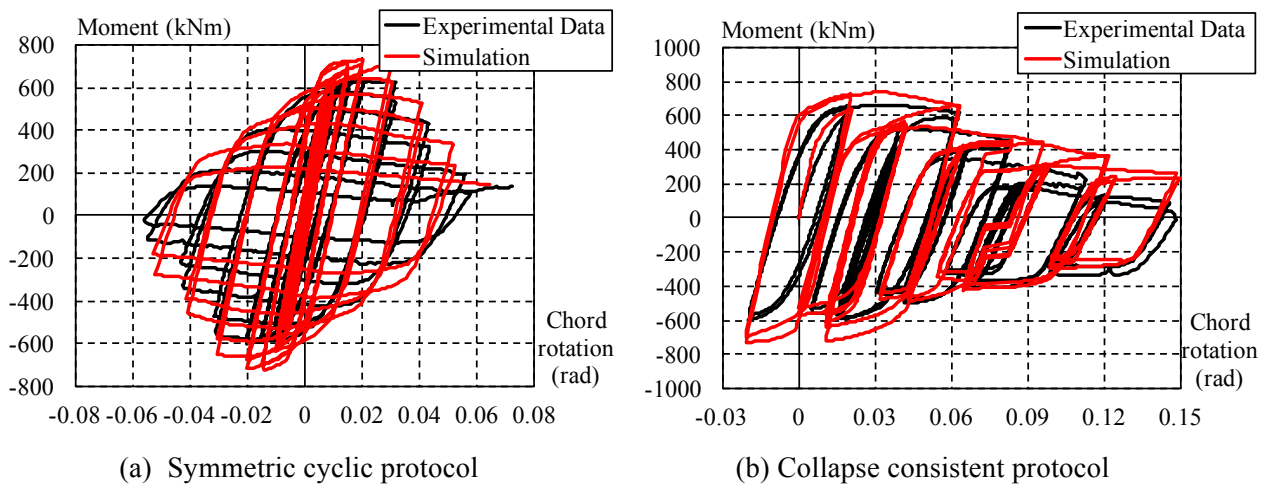


Fig. 10 – Comparison of measured versus simulated moment-rotation relations for HSS305x16 column

Figure 11 illustrates a comparison of the predicted versus measured column axial shortening – rotation relations for the HSS305x16 column. In this figure, the column axial shortening is normalized with respect to the column length. From Figure 11, the proposed steel column deterioration model is able to simulate relatively well the column axial shortening regardless of the employed lateral loading protocol. This demonstrates the potential the proposed model for earthquake-induced collapse simulations of steel frame buildings.

4. Summary and conclusions

This paper investigates the collapse behavior of steel columns as part of steel moment-resisting frames (MRFs) under seismic loading. A series of unique experiments were conducted that characterized the hysteretic behavior of nominally identical wide flange (W-shape) and hollow structural steel (HSS) columns under various lateral loading protocols coupled with constant and varying axial load ratio. The former represents the loading conditions of an interior steel column in steel MRFs. The latter is representative of end columns in steel MRFs. The tests involved 21 cantilever steel column specimens that were tested through complete loss of their flexural and/or axial load carrying capacity. The major findings of the study are summarized as follows:

- All specimens lost their flexural and axial load carrying capacity due to the formation of local buckling that developed at $0.5d$, on average, from the fixed end of a steel column. For wide flange columns a second buckling wave developed at about $1.0d$. This typically triggered lateral torsional buckling at large deformations.

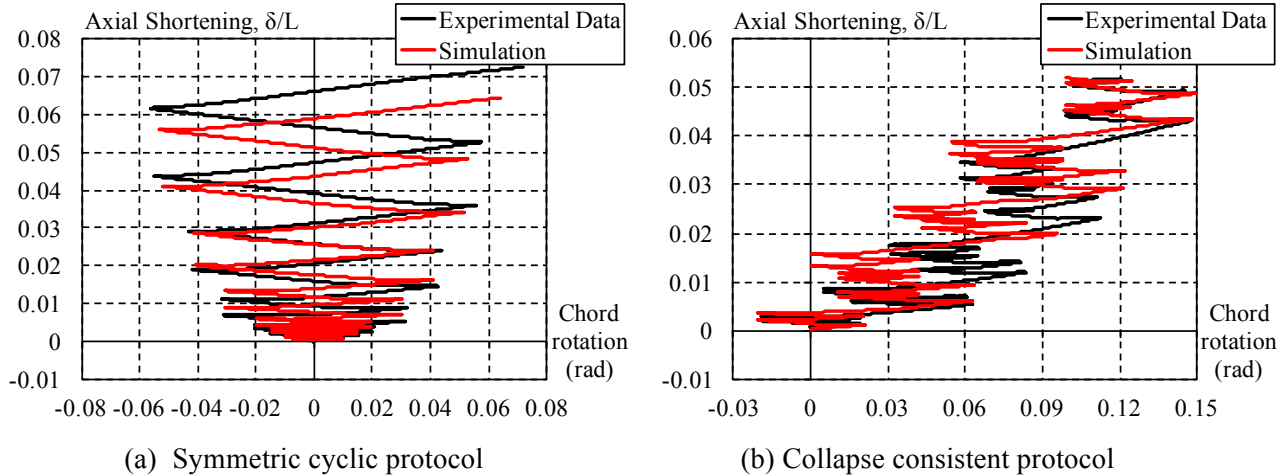


Fig. 11 – Comparison of measured versus simulated axial shortening-rotation relations for HSS305x16 column

- A dominant failure mode in all cases was column axial shortening. End columns in steel MRFs are expected to develop 6-7 times less axial shortening than adjacent columns within the same story undergoing the same lateral deformations. This is attributed to the variation of the axial load demands in end columns due to dynamic overturning effects. Therefore, differential axial shortening is likely to develop between adjacent steel columns within the same MRF story. This implies that a fully restrained beam-to-column moment connection near an end column will be subjected to both flexural and tensile axial load demands. This loading condition is currently not considered for collapse prevention of steel MRFs designed in seismic regions.
- Routinely used symmetric loading protocols do not provide the necessary information needed to realistically simulate the hysteretic behavior of steel columns at large deformations associated with structural collapse. A combination of a monotonic and a collapse-consistent loading protocol should be employed to identify the post-buckling deterioration parameters of a steel column.
- A deterioration model is proposed for simulating the hysteretic behavior of HSS steel columns. This model is based on an equivalent engineering stress-strain formulation that includes a softening branch for modeling the post-buckling behavior of an HSS column. The stress-strain relation captures the combined effect of isotropic and kinematic material hardening. The parameters of the material model can be fully defined based on standard material characterization tests. The proposed material model is employed within a fiber cross section that is assigned to a nonlinear beam-column element with a force-based formulation. It is shown that the proposed deterioration model can capture fairly well the column flexural strength deterioration as well as the column axial shortening regardless of the employed lateral loading protocol.

5. Acknowledgements

This study is based on work supported by Nippon Steel and Sumitomo Metal Corporation in Japan. The financial support is gratefully acknowledged. The authors also thank Dr. Bill Cook and Mr. Farbod Pakpour for their valuable assistance with the experimental program discussed in this paper. Any opinions, findings, and conclusions or recommendations expressed in this paper are those of the authors and do not necessarily reflect the views of the sponsors.



6. References

1. Ibarra LF, Medina RA, Krawinkler H (2005): Hysteretic models that incorporate strength and stiffness deterioration. *Earthquake Engineering & Structural Dynamics* **34**(12), 1489–1511.
2. Zareian F, Krawinkler H, Ibarra L, Lignos D (2010): Basic concepts and performance measures in prediction of collapse of buildings under earthquake ground motions. *The Structural Design of Tall and Special Buildings*, **19**(1-2), 167–181.
3. Sivaselvan M, Reinhorn A (2000): Hysteretic models for deteriorating inelastic structures. *Journal of Engineering Mechanics*, **126**(6), 633–640.
4. Lignos DG, Krawinkler H (2011): Deterioration modeling of steel components in support of collapse prediction of steel moment frames under earthquake loading. *Journal of Structural Engineering*, **137**(11), 1291–1302.
5. Lignos DG, Krawinkler H (2013): Development and utilization of structural component databases for performance-based earthquake engineering. *Journal of Structural Engineering*, **139**(8), 1382–1394.
6. Lignos D G, Krawinkler H, Whittaker A S (2011): Prediction and validation of sidesway collapse of two scale models of a 4-story steel moment frame. *Earthquake Engineering & Structural Dynamics*, **40**(7), 807–825.
7. AISC (2010): *Seismic provisions for structural steel buildings, ANSI/AISC 341-10*. Chicago, IL: American Institute for Steel Construction.
8. Suzuki Y, Lignos DG (2014): Development of loading protocols for experimental testing of steel columns subjected to combined high axial load and lateral drift demands near collapse. *10th National Conference on Earthquake Engineering*, Anchorage, Alaska: EERI.
9. Suzuki Y, Lignos DG (2015): Large scale collapse experiments of wide flange steel beam-columns. *8th International Conference on Behavior of Steel Structures in Seismic Areas (STESSA)*, Shanghai, China.
10. Lignos DG, Hikino T, Matsuoka Y, Nakashima M (2013): Collapse assessment of steel moment frames based on E-Defense full-scale shake table collapse tests. *Journal of Structural Engineering*, **139**(1), 120–132.
11. FEMA (2009): Effects of Strength and Stiffness Degradation on Seismic Response, prepared by the Applied Technology Council for the Department of Homeland Security and the Federal Emergency Management Agency, Washington, DC.
12. Elkady A, Lignos DG (2015): Analytical investigation of the cyclic behavior and plastic hinge formation in deep wide-flange steel beam-columns. *Bulletin of Earthquake Engineering*, **13**(4), 1097–1118.
13. Elkady A, Lignos DG (2016): Dynamic stability of deep slender wide-flange steel columns-full scale experiments. *SSRC, Annual Stability Conference Structural Stability Research Council*. Orlando, Florida: Structural Stability Research Council (SSRC).
14. Lemaitre J, Chaboche JL (1975): A non-linear model of creep-fatigue damage cumulation and interaction (for hot metallic structures). *Mechanics of Visco-Elastic Media and Bodies*.
15. Krawinkler H, Zohrei M (1983): Cumulative damage in steel structures subjected to earthquake ground motions. *Computers & Structures*, **16**(1–4), 531–541.
16. Yamada S, Akiyama H, Kuwamura H (1993): Post-buckling and deteriorating behavior of box-section steel members. *Journal of Structural and Construction Engineering, AIJ*, **444**, 135–143.
17. Spacone E, Ciampi V, Filippou FC (1996): Mixed formulation of nonlinear beam finite element. *Computers & Structures*, **58**(1), 71–83.
18. Scott M, Fenves G (2006): Plastic Hinge Integration Methods for Force-Based Beam–Column Elements *Journal of Structural Engineering*, **132**(2), 244–252.
19. Neuenhofer A, Filippou FC (1997): Evaluation of Nonlinear Frame Finite-Element Models. *Journal of Structural Engineering*, **123**(7): 958–966.